Elasticity of Diametrically Compressed Microfabricated Woodpile Lattices

Faezeh Shalchy* and Atul Bhaskar*

Modulus–porosity relationships are invaluable to rational material design of porous and structured solids. When struts in a lattice are compressed diametrically, the mechanics is rather complex. Herein, the problem of modulus–porosity in the spirit of scaling arguments and analyses based on simple *ansatz* followed by variational minimization of the elastic potential energy is addressed. Using scaling arguments, a simple power law where the apparent modulus of elasticity scales quadratically with the volume fraction for diametrically compressed elastic lattices is obtained. The modulus–porosity relationship is found to be consistent with computations and laboratory experiments on additively manufactured woodpile lattices with various cross-sectional shapes and lattice spacing. It is also shown that the persistence length of diametrically pinched elastic rods is small, so that the effect of compressive strain from neighboring sites can be ignored. The decay behavior is surprisingly accurately captured by the variational approach and is consistent with computations. Finally, the range of validity of the quadratic power law presented here, up to relative density ~80%, is identified. On the apparent modulus–porosity plane, the experimental data aligns well with the power law for modulus–porosity predicted from simple analyses and finite element calculations.

1. Introduction

Lattice structures and porous solids behave as materials with apparent continuum properties, when the length scale of porosity and periodicity is much smaller than the characteristic overall dimensions of the structure. Of great current interest is the apparent elasticity of such structured solids. The stress–response relationship depends on the shape and the topology of the internal architecture and properties of the parent material (see,[1] for a summary). Such analytically derived relationships exist for several lattice geometries, such as hexagonal honeycombs, or the staggered woodpile architecture, when the dominant mechanism of deformation is stretch, shear, or bending (see, e.g.,[2–5]).

A commonly encountered lattice architecture is that of elastic cylinders stacked orthogonally in alternate layers (see **Figure 1**a), we refer to this as *woodpile* lattice. We will call the horizontally running rod-like elastic structures as struts, filaments, or beads synonymously. This lattice geometry is of great current interest due to the ease of its manufacture using 3D printing, notably for use as biomedical scaffolds, where the word "beads" is frequently used to refer to extrusion. Several studies have focused on the understanding mechanics of 3D-printed structures for biomedical applications, with aim to enhance their mechanical performance as well cell activity and bone regeneration.[6–13] They utilized experiments and finite-element (FE) simulation to analyze the mechanical properties of these lattices. Consequently, there is a deficiency in studying the mechanics comprehensively. A systematic approach to understand the deformation mechanisms in structured materials is essential for designing lattices with predictable and tunable mechanical properties. The key to successfully predict the mechanical behavior of periodic structures is the identification of the dominant cell wall deformation mechanisms, for example, they could be *stretch*- or *bending*-dominated.[1,14,15] The resulting dependence of the apparent properties on the density of foams has been studied for a while (see[16,17] for early works). Studies aimed at understanding the mechanical, thermal, and electrical properties of foams have followed.[18–20]

The apparent elasticity of woodpile lattices along the two main directions of the filaments is trivial and is given by the rule of mixtures. For the stacking arrangement with alternate layers *staggered,* the compressive stiffness in the direction of stacking is

F. Shalchy
Institute of Mechanical, Process and Energy Engineering
School of Engineering and Physical Sciences
Heriot-Watt University
Scotland EH14 4AS, UK
E-mail: f.shalchy@hw.ac.uk

A. Bhaskar
Department of Mechanical Engineering
University of Sheffield
Mappin Street, Sheffield S1 3JD, UK
E-mail: a.bhaskar@sheffield.ac.uk

A. Bhaskar
Faculty of Engineering and Physical Sciences
University of Southampton
Southampton SO17 1BJ, UK

The ORCID identification number(s) for the author(s) of this article can be found under https://doi.org/10.1002/adem.202301158.
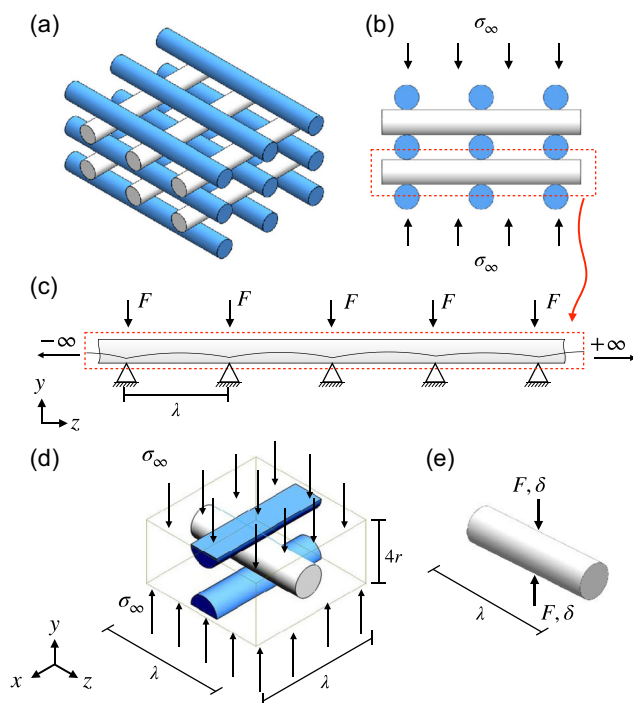
Figure 1. Schematic of a) isometric view of a woodpile lattice, b) a woodpile lattice under compression, c) a single filament loaded and supported periodically, d) unit cell of a woodpile structure in aligned arrangement under compressive loading in stacking direction, and e) a diametrically pinched elastic rod.

dominated by the flexure of the struts.[2] Bending dominated mechanics in a staggered woodpile gives rise to a fifth power relationship of modulus with porosity, that is, $E \sim \overline{\rho}^5$.[2] In contrast, when the filaments in alternate layers are stacked in an aligned arrangement (see Figure 1a), then loading the lattice remotely in the stacking direction y leads to diametrical compression. The apparent elasticity of woodpile lattices is strongly orthotropic due to the three preferred directions, of which properties along the two fiber directions are the same but different from those along the stacking direction.[3,21] Hutmacher et al.[22] reported the cellular response as well as compressive properties in the stacking direction of polycaprolactone (PCL) scaffolds fabricated using fused deposition modelling (FDM), when the alternative layers are not orthogonal. A study carried out by Ahn et al.[21] on 3D-printed dog-bone samples with aligned woodpile arrangement demonstrated that the strengths of the samples along the filaments are five times greater than that in the stacking direction. This is unsurprising and is due to the poor bonding between filaments in stacking direction.[21] Naghieh et al.[23] studied the effect of strut diameter on mechanical response of 3D-printed woodpile lattice numerically and experimentally. They developed a parametric FE model to assess the effects of layers' penetration on interlayer adhesion, which is reflected on the mechanical properties of bone scaffolds; however, there is no analytical work to compare the results against. Norato et al.[24] studied the effect of overlap between layers on the mechanical response of woodpile structures. An important feature of the problem of the diametrically pinched long cylinder,

such as those within woodpiles when compressed in the stacking direction, is that it is neither a case of plane stress nor plane strain. Although the cylindrical struts are long, as required for plane strain, the diametrical compression is at a point along the length and not all along the length as a line load. Likewise, a thin disc compressed diametrically would be acceptable for analysis using plane stress approximation, but the long struts do not allow this approximation to be valid either. Norato et al.[24] considered deformation of pinched cylinders due to remote compression as a linear combination of the deformations due to the two extreme cases of planar elasticity. While they provide an expression for the apparent stiffness as a function of the geometrical and material parameters, the relationships are rather complex and use a combination of plain stress and plain strain.

Woodpile lattices are of particular interest in tissue engineering. The effect of the relative position of the filament with respect to adjacent layers on the apparent properties of woodpile scaffolds under compression was first studied by Sobral et al.[25] experimentally. Arrangements that possessed staggered placements of filaments showed superior results for cell growth. Yeo et al.[26] reported that changing the relative position of the filaments produces different pore sizes that results in scaffolds more suitable for bone tissue engineering applications. Yazdanpanah et al.[13] suggested that they noticed for the first time that the mechanical properties of aligned and staggered scaffolds are very different. While certain studies have suggested that aligned woodpile scaffolds demonstrate superior mechanical properties, others have found no distinction between aligned and staggered scaffolds in terms of elastic modulus. Varied correlations between porosity and mechanical properties seem to account for these discrepancies. Hence, there is an urgent need to study the mechanical properties of such lattices systematically. In the longer term, such studies would provide guidelines for designing and fabricating aligned and staggered scaffolds to replicate the mechanical properties for trabecular bone. While motivation of this work arises from tissue engineering scaffolds, there are other potential applications where porous solids and solid foams are used. This study is primarily of mechanical nature and it is valid regardless of the biomedical properties of matter such as biocompatibility–which relates to the cellular response to foreign material, bioresorbability, biodegradability, etc. We acknowledge that while these may be serious concerns for practical applications in biomedical engineering, here we restrict our attention to the mechanical response alone. There are other potential applications of such elastic lattices in nonbiological contexts such as their potential use for elastic or vibroacoustic metamaterials. The main requirement for the applicability of the results presented here is the diametrical compression of the struts as the dominant mechanism of deformation and the validity of the linear constitutive laws.

Although some aspects of the mechanics of woodpile structures with cylindrical struts have been investigated in the past,[27,28] a systematic study on mechanics of aligned arrangement and the effect of strut cross-section shapes on their mechanical properties is currently missing.

It is sometimes possible to obtain a power law relating the apparent modulus to the porosity, when such relationships exist, and when simple analysis is possible. As opposed to cell walls within a cellular solid undergoing bending or stretch

deformations mentioned earlier, the present work is concerned with a complex situation because the dominant mechanism is diametrical compression. This is a significantly harder problem mathematically, yet here we approach the problem in the spirit of simple analysis–enabled by a scaling argument. Further, the effect of compression at the neighboring sites is assessed and found to be negligible for spacing greater than the diameter. Again, an elegant analysis to estimate the persistence length of pinching of an elastic cylinder is found to match extremely well with numerical simulations, thus justifying the approximation that we can ignore the response arising from compression at the neighboring lattice sites.

Here we develop a power law relationship for the apparent elasticity of such lattices theoretically and verify the same computationally and experimentally. Following this, an ansatz of decaying elastic response is proposed, in which the unknown exponent is treated as the generalized coordinate of the problem that is subsequently determined by variational minimization of the total potential energy. The persistence length of pinching of an elastic cylinder turns out to be short enough that enables ignoring the compression at nearby lattice sites. Results from FE simulations and laboratory experiments are found to be consistent with the simple power law presented here.

2. Theoretical and Computational Analysis of the Apparent Stiffness

Theoretical analysis for lattice materials, when possible, may lead to power law relationships between the apparent stiffness and the porosity, the results for which are sparse. Here the dominant mechanism of elastic deformation is the diametrical compression of cylindrical struts. Such pinched cylinders are analytically intractable, as the situation is neither of plane stress nor plane strain. Since we know that the response of such pinched solid cylinders is localized, with rapidly decaying displacement field, here we develop a theory for diametrically compressed lattices by 1) employing a scaling argument in the linear elasticity regime; and 2) showing that the effect of compression at nearby lattice sites is negligible. Scaling analysis cannot provide the value of the constant C mentioned later in this article. FE simulation has been utilized to identify the C constant.

2.1. Modulus–Porosity Relationship: Scaling Argument

A remote compressive stress is applied in the stacking direction of woodpile lattice with alternative layers aligned (see, Figure 1b). The deformation in such elastic lattices is due to diametrical compression. The interaction between these layers is complex. Localized response would, in principle, follow contact mechanics, which is known to be nonlinear because contact area depends on loading. Such localized response is out of our consideration presently. Here we are interested in the apparent Young's modulus of such lattices in the stacking direction, an idea necessarily associated with linear elastic response. Each filament is modeled as a periodically pinched elastic cylinder (see, Figure 1c). A unit cell under transverse stress is shown in Figure 1d. The apparent compressive strain in the loading direction is given by the ratio of the transverse compression 2δ and the transverse length $4r$ over

which the compression takes place (see Figure 1d). The unit cell contains two diameters (one whole and two halves). The diametrical compression for the unit cell is 2δ whereas it is δ per cylinder. The apparent remote stress σ_∞ can be related to the pinching force F, as shown in Figure 1e. The apparent stress and strain are thus respectively given by

$$\sigma_\infty = \frac{F}{\lambda^2} \quad \text{and} \quad \langle \varepsilon \rangle = \frac{2\delta}{4r} \tag{1}$$

where λ is the lattice spacing. The apparent modulus of elasticity is, therefore, given by $\langle E \rangle = \sigma_\infty / \langle \varepsilon \rangle$. Substituting this into Equation (1), apparent Young's modulus is given by

$$\langle E \rangle = \frac{2Fr}{\delta\lambda^2} \tag{2}$$

An analytical relation between F and δ is required to close the problem.

The functional form involving geometrical and material parameters in the $F - \delta$ relationship for linear response can be developed by a simple scaling argument using the well-known Buckingham Pi theorem.[29,30] For the deformation of a solid rod under two diametrically opposing point loads, Young's modulus of the parent material, Poisson's ratio, diameter, and the applied force are the relevant variables. This results in the three nondimensional numbers $\Pi_1 = F/Er^2$, $\Pi_2 = \delta/r$, and $\Pi_3 = \nu$. The force–displacement relationship can then be expressed as

$$\frac{\delta}{r} = \phi\left(\frac{F}{Er^2}, \nu\right), \quad \text{or} \quad \frac{\delta}{r} = \left(\frac{F}{Er^2}\right)^m (\nu)^n \tag{3}$$

where m and n are unknown exponents. For linear response, $\delta \propto F$, so the function ϕ must factorize with $m = 1$. Also, the role of Poisson's ratio is often not significant and can be absorbed in the proportionality constants. Therefore,

$$\delta \propto \frac{F}{Er} \tag{4}$$

The constant of proportionality can be established by computation or physical experiments. The volume fraction is given by $\bar{\rho} = (\pi r/2\lambda)$. Substituting the $F - \delta$ relationship from Equation (4) into Equation (2), the apparent Young's modulus as a function of volume fraction $\bar{\rho}$ is given by

$$\langle E \rangle = CE\bar{\rho}^2 \tag{5}$$

where C is a nondimensional constant that can be determined by detailed analysis, computations, or experiments. The simplicity of the power law with a quadratic exponent is appealing. Indeed, such power laws, when they exist, provide interesting insight into the dependence of the behavior in a simple and usable form.

The relationship obtained above is valid for noncylindrical cross-sectional shapes too, with a characteristic length of the cross section in the direction of compression, say χ, replacing the radius. Hence, for lattices with struts of square cross section of side a or hexagonal cross section with distance between flats b, we can write

$$\delta_\square \propto \frac{F}{Ea}, \quad \text{or,} \quad \delta_\bigcirc \propto \frac{F}{Eb} \tag{6}$$

The modulus–porosity relationship for lattices with other cross-sectional shapes would again be a power law as in Equation (5), except that the constant of proportionality would depend on this shape.

2.2. Persistence Length of a Pinched Elastic Rod

The above analysis assumes an infinite cylinder pinched at a single diametrical location. In reality, a pinched strut suffers compression that could potentially impact the apparent strain at the *neighboring lattice sites*. We will call the decay length scale associated with the axial response to pinching as the persistence length. The term persistence is usually associated with the bending stiffness of a polymer, given by its ratio with the Boltzmann constant $k_B T$. Here we will use the term in the spirit of describing a decay length associated with localized pinching. Recently such persistence lengths for hollow cylinders[31] and for thin elastic strips[32] have been studied. In a lattice, the influence of neighboring points must be accounted for, only if it is significant.

We estimate the persistence length variationally using a simple ansatz. The approach is deliberately kept simple in order to estimate the role of local deformation on neighboring sites. The axial decay is assumed to be exponential, which is consistent with the well-known Saint-Venant's principle, which states that the effect of self-equilibrating system of forces away from their point of application decays rapidly. Consider an infinitely long elastic rod, pinched at the origin $z = 0$, as shown in **Figure 2**a. The strain energy in a deformed elastic solid is given by the volume integral

$$U = \frac{1}{2}\int \sigma_{ij}\varepsilon_{ij}\,dV \tag{7}$$
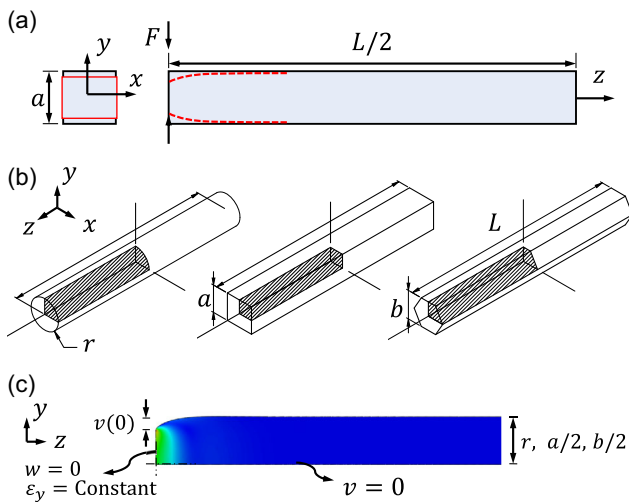

(a)

(b)

(c)

Figure 2. a) Schematic diagram of pinched rod of square cross section. b) Three different cross-sectional shapes: circular with the radius r, square of side a, and hexagonal of height b. Symmetry allows modeling only one-eighth of the structure to be modeled. c) Prescribed displacement field consistent with constant strain is applied at the face $z = 0$.

where summation is implicit over the repeated indices. Direct stresses in the x- and z-directions as well as shear in the $x - y$ plane are negligible when the rod is pinched in the y-direction (see Figure 2), that is, $\sigma_{xx} = \sigma_{zz} = \tau_{xy} \approx 0$. The displacement in the z-direction is negligible, that is, $w \approx 0$. We further assume that strain energies due to shear deformation in the $x - z$ plane are also small, as they are due to Poisson coupling. The validity of these simplifications will be assessed numerically.

Consider an ansatz $v(x, y, z) = qye^{-\beta z}$ with two undetermined parameters q and β. The nonzero strain components required to evaluate the strain energy can be calculated as

$$\varepsilon_{yy} = \frac{\partial v}{\partial y} = qe^{-\beta z}, \quad \gamma_{yz} = \frac{\partial v}{\partial z} + \frac{\partial w}{\partial y} = -\beta qye^{-\beta z} \tag{8}$$

The total strain energy expression now simplifies to

$$U = \frac{1}{2}\int \left(\varepsilon_{yy}\sigma_{yy} + \tau_{yz}\gamma_{yz}\right)dV \tag{9}$$

Substituting $\sigma_{yy} = E\varepsilon_{yy}$ and $\tau_{yz} = G\gamma_{yz}$, the energy associated with compression and shear can be written as

$$U_{\text{comp}} = \frac{1}{2}\int E\varepsilon_{yy}^2\,dV \quad \text{and} \quad U_{\text{sh}} = \frac{1}{2}\int G\gamma_{yz}^2\,dV \tag{10}$$

For filaments of constant cross-sectional area A, $dV = A\,dz$. Substituting for strain and integrating over z from zero to infinity, U_{comp} and U_{sh} are analytically obtained as

$$U_{\text{comp}} = \frac{1}{2}\left(\frac{EAq^2}{2\beta}\right) \quad \text{and} \quad U_{\text{sh}} = \frac{1}{2}\left(\frac{GA\beta a^2 q^2}{24}\right) \tag{11}$$

Both expressions are quadratic in the amplitude parameter q. After using the relationship between shear modulus and the Young's modulus, via the Poisson's ratio, we have

$$U = \frac{q^2 EA}{4}\left(\frac{1}{\beta} + \frac{a^2\beta}{24(1+\nu)}\right) \tag{12}$$

The dependence of U on β within the two terms is competing because the strain energy due to diametrical compression is $\sim \beta^{-1}$, whereas that due to shear is $\sim \beta$. Equilibrium is a result of the competition between these two energy terms that is resolved by variationally minimizing U with respect to β. Using the principle of minimum potential energy, that is, $\delta U = 0$, δ represents the first variation, we assert $\partial U/\partial\beta = 0$. So, we analytically obtain $a\beta = \sqrt{24(1+\nu)}$, which shows weak dependence on the Poisson's ratio of the order of $\nu/2$. For $\nu = 1/3$, we have $\beta = 4\sqrt{2}/a \approx 5.66 \times a^{-1}$. Hence, displacement in y-direction that characterizes axial persistence is given by $v(x, y, z) = qye^{-5.66(z/a)}$. An upshot of the simple analysis is that we have an estimate of axial *propagation* of the pinch to other nearby locations in a lattice. The pinching action takes place at a spatially periodic interval. For example, the axial displacement at a distance a away from the location of pinching would be $e^{-5.66} = 0.35\%$ of what it is where the rod is pinched. So, we can safely ignore the effect of axial propagation of compression to nearby locations and the lattice response would be adequately

2301158 (4 of 9)

represented by just the local compression of an infinitely long pinched filament. The simple analysis is validated against FE simulations in the following section.

The effect of pinching at sites further away is progressively less. The simplicity of the analysis gives us an estimate that is independent of the *shape* of the cross-section. Of course this would not be the case in a detailed elasticity solution. However, we made a deliberate choice of simplifying the energy terms and estimating if the effect of pinching at neighboring pinched sites needs to be accounted for. The apparent modulus of elasticity versus porosity is the main motivation of this work, as the power law Equation (5) provides a simple and useful relationship for material design, which a detailed account of a higher-order effect would compromise. The efficacy of the simplifications in estimating the persistence of diametrical pinching is assessed computationally in the following section.

2.3. Diametrically Pinched Elastic Rods: Computational Assessment of Persistence

The spatial decay of the elastic response can be computationally estimated for various geometries. Constant strain in the pinching direction is applied to sufficiently long rods by imposing the displacement field through the cross section as per $v(x, y, 0) = qy$, as in the previous analysis. The commercial code ABAQUS/CAE/Standard 6.18 (Simulia, Dassault Systèmes, Providence, RI, USA)[33] was used for simulating the pinching deformation. Three different shapes of the cross section of the rod are considered. Because of the three planes of symmetry in the problem, only one octant of the structure needs to be modeled as shown for the circular, square, and hexagonal cross sections (Figure 2b). Boundary conditions are applied respecting these symmetries so that all the nodes on the left and bottom edge remain in their plane; see Figure 2c. Displacement $v(x, y, 0) = qy$, consistent with constant strain over the cross section, that is, $\varepsilon_{yy}(x, y, 0) = q$, is applied. The computational model thus set up provides estimates of persistence due to imposed displacement field. Mesh refinement was carried out to ensure convergence. Here we consider persistence under extreme situations: 1) plain strain when the depth in the x-direction is large so that the problem becomes one of thin layer being squeezed in the thickness direction; 2) plain stress when the depth in the x-direction is small compared to the thickness; and 3) when the $x - y$ cross section is square. The deformation $\bar{v} = v/\chi$, as a function of $\bar{z} = z/\chi$, shows very similar roll-off profiles for the three cases (in **Figure 3**a). Here $\chi = 2r$, a, or b is the characteristic length in the y-direction. The persistent length, the distance at which the response reduces to $1/e$ of it its value, is estimated as $\ell_p = \beta^{-1} \approx 0.18 \times a$ for a square section of side a, as the slope of -5.6 in Figure 3b is close that from the simple theory. The periodic dips are associated with a change in sign of v in the oscillatory response obtained from FE simulations, so that logarithmic response shows sharp dips. A similar oscillatory response due to pinching has been reported for hollow shells in refs. [31,34] and is associated with complex exponents and potentially two length scales if the real and the imaginary parts are different. The simple analysis presented here does not bring out these subtle features, but is adequate for the purpose. Results from FE simulations of rods with cross section of three different
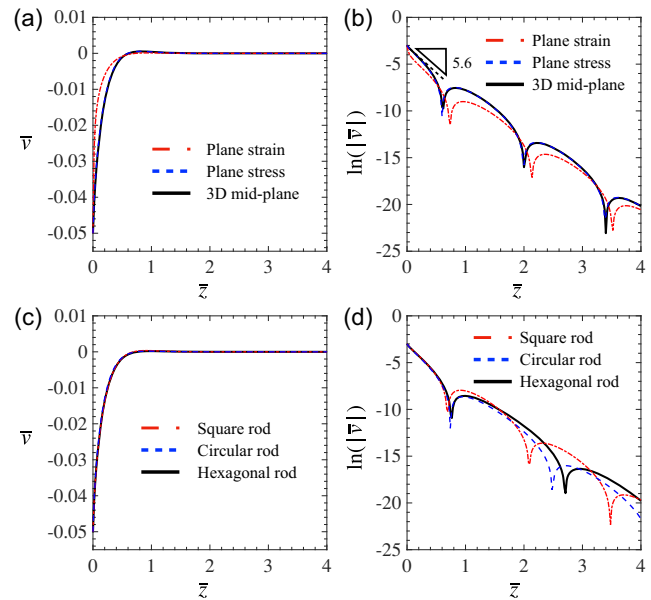

Figure 3. The deformation of compressed rod obtained from FE for different element types (plane stress, plane strain, and 3D elements (ten-node tetrahedral -C3D10)) and rods with various cross-sectional shape. a,c) Displacement in y-direction (v) versus the length of filament. b,d) Log of the absolute value of displacement in y-direction (v) versus the length of filament.

shapes under constant imposed strain $\varepsilon_{yy} = q$ are shown in Figure 3c,d. The persistent length for rods with hexagonal and circular cross section is estimated to that for a square cross section. The deformation profile decays as per $\exp(-5.6\bar{z})$, where $\bar{z} = z/\chi$, depending on the shape of the cross section. The simple theory presented here provides decay rates close to those previously reported using very detailed analysis for hollow cylinders specialized for solid cross section[35] which gives $kb = 2.8$, that is, $k = 2.8 \times b^{-1}$, where b is the radius, rather than diameter, which means a decay rate of -5.6 in our notations. For solid cylinders, see;[36] the value of decay rate (reported there as -5.586, for $\nu = 0.25$) is again very close to our estimates. Since the persistence length is smaller than the cross-sectional characteristic length χ, as shown in this and the previous subsection, we expect that the modulus–porosity relationship $\langle E \rangle = C E \bar{\rho}^2$ obtained from a diametrically compressed infinitely long strut would be close to one for lattice with finite spacing. This is taken up computationally and experimentally, and results are presented in the following sections.

2.4. Apparent Modulus for an Elastic Lattice: Computations

The power law (5) is now reconciled against computations. A unit cell is modeled within the ABAQUS environment. A *prescribed vertical displacement* is applied at all the nodes of the top surface of the unit cell. The nodes on the bottom surface are constrained in all degrees of freedom, while due to periodicity of the structure, all the nodes lying on the vertical surfaces are constrained to remain in their plane, allowing displacements in that plane. Filaments in lattices are modeled as elastic cylinders and meshed

**ADVANCED
SCIENCE NEWS**

www.advancedsciencenews.com

**ADVANCED
ENGINEERING
MATERIALS**

www.aem-journal.com

using ten-node tetrahedral (C3D10) elements that use quadratic interpolation. The material properties assigned are Young's modulus, $E = 2290\,\text{MPa}$[28] and Poisson's ratio, $\nu = 0.36$.[37] The smallest element size in FE mesh is 0.05 mm.

The bonding between filaments was modeled by considering an overlap in the volumes of adjacent cylinders. Unit cells are modeled considering the woodpile structure with 15% overlap between layers, similar to the 3D-printed lattices discussed in the following section. The apparent density ($\overline{\rho}$) is calculated both geometrically and using the mass property calculation tool within ABAQUS. The diameter of the cylinders was taken as $2r = 0.25$, 0.40, 0.60, and 0.80 mm. These correspond to the size of commercially available FDM nozzles. Center-to-center separation between the filaments λ was varied systematically across samples manufactured for compressive testing, to obtain a range of the porosity and study its relationship with the apparent properties. By varying λ, while keeping the filament diameter fixed, porous lattices of varying relative density, $\overline{\rho}$, were simulated under compressive load in the stacking direction.

The contrast between the modulus–porosity relationship for the aligned versus the staggered stacking is apparent in **Figure 4**. While the staggered stacking obeys a fifth-power dependence of the apparent modulus on relative density $\overline{\rho}$, as reported previously in,[2] the diametrically compressed aligned woodpile shows a scaling $\langle E \rangle \sim \overline{\rho}^2$. The deviation for the computationally obtained modulus–porosity relationship from a fifth-power line is attributed to shear combined with bending for short overhang (see, Cuan et al.[2]). Moreover, the validity of the fifth-power law is restricted to high-porosity region in addition to ignoring shear and higher-order deformations. On the other hand, numerical simulations are extremely close to the power scaling for diametrically compressed woodpiles, given by Equation (5). The highest achievable density for woodpile lattices with noncontacting struts is when $\lambda = 2r$, that is, $\overline{\rho} = \pi/4 \approx 78.5\%$. Thus the quadratic power law would start significantly deviating from the power law presented here. We carried out numerical simulations for the whole range of apparent density. As expected, both graphs approach $\langle E \rangle / E = 1$ for solid material ($\overline{\rho} = 1$), the shaded area

shows the region of inapplicability of the simple power law, which coincides closely with $\overline{\rho} > \pi/4$.

It is sometimes possible to obtain simple relationships using scaling arguments (see e.g., Gibson and Ashby,[1] Warner and Edwards[14] in the context of solid foams). Planar honeycombs and open cell 3D foams show $\langle E \rangle \sim \overline{\rho}^3$ and $\langle E \rangle \sim \overline{\rho}^2$ scaling respectively, because bending mechanics entails $\sim t^3$ and $\sim t^4$ scaling for flexural stiffness whereas the volume fraction scales as $\overline{\rho} \sim t$ and $\overline{\rho} \sim t^2$ for the two cases respectively, t being the cell wall thickness. Similarly stretch dominated planar honeycombs, for example, triangular lattice of struts, the modulus–porosity scaling is $\langle E \rangle \sim \overline{\rho}$, because stretch stiffness and volume fraction both scale as $\overline{\rho} \sim t$. Staggered woodpiles are again bending dominated, if the lattice separation is large, compared to the diameter. The bending stiffness scales as per r^4/λ^3, remote stress as per $\sigma_\infty \sim \lambda^{-2}$, apparent strain as per $\langle \varepsilon \rangle \sim r^{-1}$, whereas the volume fraction follows $\overline{\rho} \sim \lambda/r$, giving rise to $\langle E \rangle \sim \overline{\rho}^5$. Such power laws are based on simple mechanics of slender rods. The mechanism of diametrical pinching, by contrast, is rather complex and hence not amenable to simple analysis. Our scaling argument presented here shows a quadratic power law $\langle E \rangle \sim \overline{\rho}^2$ for aligned woodpile lattices under *diametrical compression*, the basis of which is Equation (1)–(5).

2.5. Modulus–Porosity Relationship: Laboratory Experiments

Additive manufacturing affords the possibility of tailoring the porosity of woodpile lattices by controlling the spacing of the struts as well as using different diameters for the nozzle used for dispensing the material. This was achieved by a bespoke sequence of machine instructions as G-code used to control the movement of print tool. Ultimaker² Extended+ is used to fabricate the specimens by FDM 3D printing method. All specimens were fabricated at 205 °C with speed of 1000 mm min⁻¹ and fan speed of 80%. Nozzle with square bore manufactured[38] as well as the available standard nozzles are used to fabricate woodpile lattices. Scanning electron micrscopy (SEM) micrographs of cross section of woodpile structures printed with circular nozzle of 0.4 mm radius and square nozzle of 0.53 mm side length are shown in **Figure 5**. There is a deviation of the diameter of the extruded filaments from the nominal nozzle diameter, which is estimated to be less than 9%. As expected, there is flattening of the extrusion so that the diameter is slightly wider horizontally and slightly shorter vertically, resulting in ellipticity of a small degree. Our measurements for printed samples using 0.4 mm nozzles show horizontal and vertical diameter of the fabricated extrusions as (410 ± 16) and $(379 \pm 13)\,\mu\text{m}$, respectively. These measurements for the square nozzle of 0.53 mm nominal side length are (567 ± 17) and $(500 \pm 11)\,\mu\text{m}$, respectively. The variance is due to inevitable variability in the fabrication process, whereas difference in the mean vertical dimensions versus that in the horizontal direction is due to flattening of the molten material during solidification, which is a systematic deviation from the intended geometry. The relative densities of specimens are calculated using the total weight, the material density, and the total external volume of the printed cubic samples. The length and width of compression test specimens are chosen according to the ASTM standard D1621 to be 50 mm × 50 mm and their
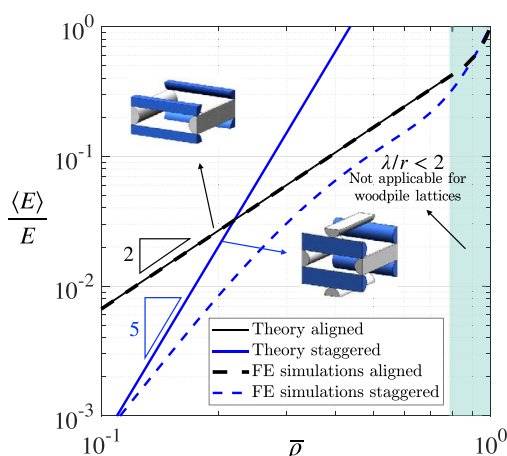

Figure 4. Comparison between the apparent modulus of aligned and staggered woodpile lattices, theory, and FE simulations. The shaded area shows the limit of applicability when struts start contacting at $\overline{\rho} = \pi/4$.
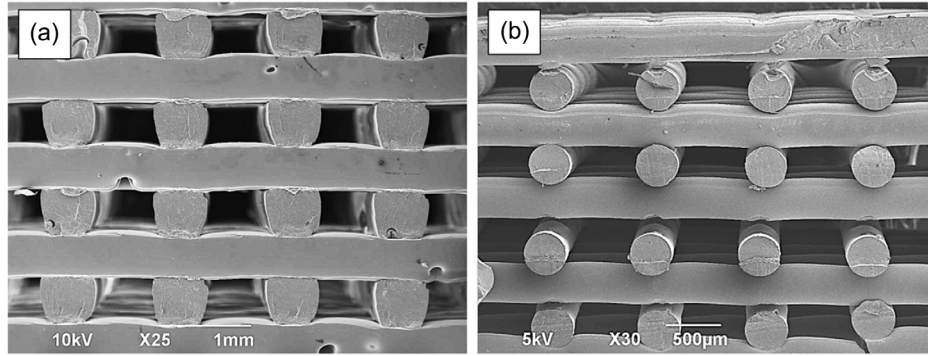
Figure 5. SEM micrograph of FDM-fabricated aligned woodpile structures with a) square nozzle with the side length of 0.53 mm and b) circular nozzle with diameter of 0.4 mm nozzles. The deviation in the diameter of the extruded filaments from the nominal nozzle diameter is less than 9%.

height is ≈25 mm. Instron 5569 was used to perform the uniaxial compression tests with strain rate of $3 \times 10^{-4}\,\text{s}^{-1}$. Dino-lite microscope is used to capture images during the tests.

3. Results and Discussion

The apparent Young's modulus is the ratio of the remote stress and the apparent lattice strain. The applied remote stress σ_∞ is obtained from computations by dividing the total reaction force by the area of the unit cell, $A = \lambda^2$, whereas the applied vertical displacement is divided by the original height of the unit cell in the loading direction, that is, $\approx 4r$, to obtain the apparent strain in the lattice $\langle \varepsilon \rangle$. Apparent Young's moduli thus calculated from simulations is plotted as a function of relative density for circular and square strut cross sections in **Figure 6**. The apparent Young's modulus scales as $\langle E \rangle \propto (\overline{\rho})^2$ for both arrangements, as predicted by our analysis; see Equation (5). For $\overline{\rho} = 1$, which is when the lattice turns to a solid block, the apparent Young's modulus will reach to value of $\frac{\langle E \rangle}{E} = 1$. A parabolic asymptote is fitted to the FE
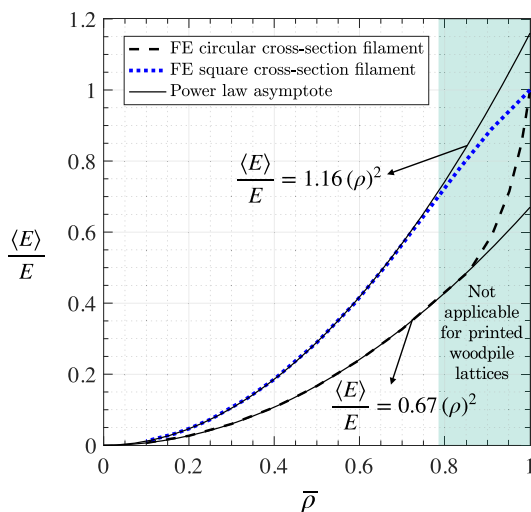
simulation results for the small densities using data points at low $\overline{\rho}$ values of the data from FE calculations. The exponent of the fitted power law is strikingly close to the predicted value of 2. The constant of proportionality from the two shapes of the cross section are different—a steeper parabola for the lattice with square cross-section struts, whereas a shallower one for that with circular cross section. In both cases, FE simulation results depart from the power law for values of the relative density greater than ≈0.8. For lattices with square cross-section struts, FE calculations show a falling slope at the denser end of the plot, whereas in the trend for structures with circular cross section, a rising slope is observed.

For lattices with struts of circular cross section, the results fit to a power law $\langle E \rangle / E = C(\overline{\rho})^2$ in which $C \approx 0.67$ for 15% overlap in FE simulations. The power law coefficient weakly depends on the layer overlap. This effect is not studied here but it has been studied theoretically and numerically by Norato et al.[24] For lattices with struts of square cross section, the results fit a power law of $\langle E \rangle / E = B(\overline{\rho})^2$ with $B \approx 1.16$.

The compressive response of lattices were studied experimentally next. The power law dependence, as presented earlier in Figure 6, is brought out best on a logarithmic scale, where the trend should be linear with a slope 2. Predictions from scaling argument based on power law and well as FE results (in Figure 6) are compared with experimental values of the modulus (derived from tests such as those in **Figure 7**) an are now overlaid on a single graph in **Figure 8**. Samples with different filament diameters, spacing between filaments, and a fixed layer overlap of ≈15% were 3D printed and tested. Two typical stress–strain curves obtained experimentally are presented in Figure 7. The stress–strain curve of these samples starts with a linear elastic part, followed by a plateau due to yielding of the material, leading eventually to material densification. At least three identical specimens are tested for each combination of lattice spacing and strut diameter. Similar trends are observed in specimens with square cross-sectioned filaments. However, due to the high contact area, the stiffnesses of these specimens are higher than specimens with circular cross-sectioned rods. Young's modulus was obtained for each sample from stress–strain curves such as those in Figure 7. A dot on Figure 8, with error bars showing variability in measurement, represent the apparent modulus value thus obtained for each lattice with a chosen spacing and strut
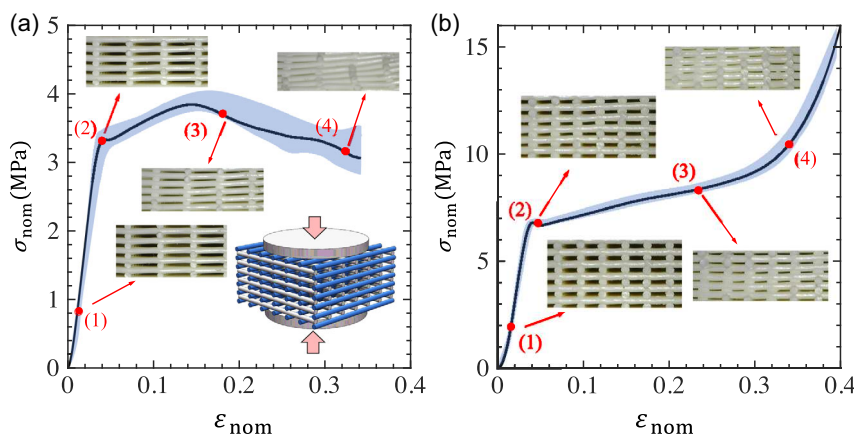

Figure 6. Apparent modulus versus apparent density of a woodpile structure with struts of cylindrical and square cross sections. The shaded area refers to $\overline{\rho} > \pi/4$, when struts start contacting each other.

**ADVANCED
SCIENCE NEWS**

www.advancedsciencenews.com

**ADVANCED
ENGINEERING
MATERIALS**

www.aem-journal.com

Figure 7. Stress–strain curve for two set of identical specimens with aligned woodpile arrangement under compression a) $r = 0.2$ mm and $\lambda = 2.4$ mm and b) $r = 0.3$ mm and $\lambda = 1.6$ mm.
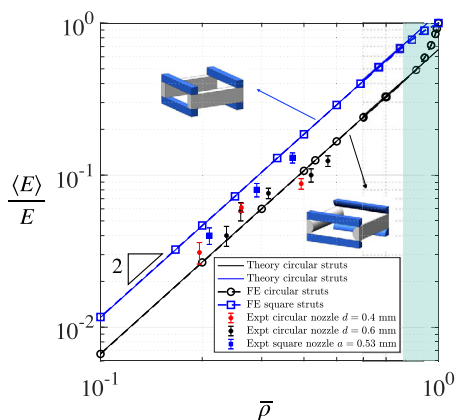

Figure 8. A comparison results for the apparent Young's modulus versus apparent density between the experimental and those obtained from FE simulations, alongside the predictions from the simple theory, considering woodpile structures with struts of square and cylindrical (15% overlap) cross-sectioned filaments.

diameter. The two trend lines in this figure show a linear dependence with slope 2, confirming the anticipated quadratic power law, consistent with the scaling argued earlier.

A comparison between experimental results for the apparent Young's modulus with those from FE simulations as well as the simple theory (Section 2) for woodpile structures with struts of circular and square cross sections is presented in Figure 8. Results from FE calculations are shown using circular and square markers with a dashed line. Trends from the simple theory are presented using solid lines that overlap with FE calculations for much of the lower range of porosity, and the departure is only at the very high end of porosity within the shaded band at the right end, as expected. Nozzles of two different diameter and a *bespoke nozzle with square outlet* were used to print woodpile lattices with various center-to-center spacing in order to obtain lattice structures of a range of porosity values. The apparent modulus for each layer-wise additively manufactured structure is presented on the modulus–porosity plane using dots

with experimental error bars. The apparent Young's modulus scales as $\langle E \rangle \propto (\overline{\rho})^2$, as predicted by our analysis; see Equation (5). The trend is along straight lines, with slope 2, on a double-log graph on the modulus–porosity plane. Straight lines with slope 2 on a log–log plot in Figure 8, as obtained from FE calculations, confirm this. The apparent modulus of specimens with square cross section is higher than that for specimens with circular struts for a given porosity. This effect is more pronounced in FE calculation. Note that the simple theory enunciated via Equation (5) here provides the quadratic dependence on volume fraction and linear scaling with the Young's modulus, but the constant C, which depends on the cross-sectional shape, has to be obtained from another analysis or experimentation, here we have used the power law fit (Figure 6) with FE to determine this cross-sectional shape-dependent constant. The vertical shift in the straight lines reflects this difference in the value of the constant of proportionality.

4. Conclusion

We present a power law relationship between the apparent modulus of elasticity along the stacking direction, and the porosity of a woodpile lattice, when struts are diametrically compressed. A simple scaling argument results in the modulus being proportional to the second power of the relative density, which is found to be consistent with our computations and laboratory experiments. The modulus–porosity relationship presented here is based on the diametrical compression of a long elastic rod, which suggests effects of compressive response from neighboring sites. We demonstrate using a simple analysis that the persistence length of a pinched solid rod is comparable to the cross-sectional characteristic length, so that the effect at about one cross-sectional distance is of the order of 3%–4% and hence can be ignored. That such a diametrical compression is localized is further verified computationally. Lattice structures of varying porosity were fabricated using additive manufacturing, so that the modulus–porosity relationship could be experimentally observed. This was achieved by 1) *controlling the lattice spacing*; 2) and *using nozzles with different bore size*, including a bespoke

nozzle capable of dispensing beads of square cross section. For dense staggered woodpile lattices, the deviations from the power law are expected and can be attributed to unaccounted for deformations. The experimental modulus–porosity relationship agrees well with detailed FE simulation. An implication of the present work is in advanced material design that is enabled by a simple power law with respect to porosity, despite rather complex inherent mechanics in the diametrical compression.

Conflict of Interest

The authors declare no conflict of interest.

Data Availability Statement

Research data are not shared.

[1] L. J. Gibson, M. F. Ashby, in *Cellular Solids: Structure and Properties*, Cambridge University Press, Cambridge, UK **1997**.

[2] E. Cuan-Urquizo, F. Shalchy, A. Bhaskar, *Int. J. Mech. Sci.* **2020**, *187*, 105932.

[3] G. Ye, H. Bi, L. Chen, Y. Hu, *3D Print. Addit. Manuf.* **2019**, *6*, 333.

[4] S. Raghavendra, A. Molinari, V. Fontanari, M. Dallago, V. Luchin, G. Zappini, M. Benedetti, *Proc. Inst. Mech. Eng., Part C* **2020**, *234*, 3241.

[5] H. Liu, L. Chen, B. Du, S. Peng, Y. Guo, Y. Zhao, L. Chen, H. Zhou, W. Li, P. Liu, *Compos. Struct.* **2019**, *210*, 118.

[6] T. D. Ngo, A. Kashani, G. Imbalzano, K. T. Nguyen, D. Hui, *Compos. Part B: Eng.* **2018**, *143*, 172.

[7] E. O. Bachtiar, O. Erol, M. Millrod, R. Tao, D. H. Gracias, L. H. Romer, S. H. Kang, *J. Mech. Behav. Biomed. Mater.* **2020**, *104*, 103649.

[8] A. Entezari, J. Fang, A. Sue, Z. Zhang, M. V. Swain, Q. Li, *Mater. Lett.* **2016**, *184*, 108.

[9] M. de Wild, S. Zimmermann, J. Rüegg, R. Schumacher, T. Fleischmann, C. Ghayor, F. E. Weber, *3D Print. Addit. Manuf.* **2016**, *3*, 142.

[10] Q. Yan, H. Dong, J. Su, J. Han, B. Song, Q. Wei, Y. Shi, *Engineering* **2018**, *4*, 729.

[11] D. O. Cohen, S. M. Aboutaleb, A. W. Johnson, J. A. Norato, *J. Mech. Des.* **2021**, *143*, 121701.

[12] X. He, Q. Zhao, N. Zhang, J. Wang, Q. Si, Y. Xue, Z. Xing, *J. Appl. Biomater. Funct. Mater.* **2023**, *21*, 22808000231181326.

[13] Z. Yazdanpanah, N. K. Sharma, A. Raquin, D. M. Cooper, X. Chen, J. D. Johnston, *BioMed. Eng. Online* **2023**, *22*, 73.

[14] M. Warner, S. Edwards, *Europhys. Lett.* **1988**, *5*, 623.

[15] P. Chopra, PhD thesis, University of British Columbia, **2011**.

[16] A. Gent, A. Thomas, *J. Appl. Polym. Sci.* **1959**, *1*, 107.

[17] R. Duckett, S. Rabinowitz, I. Ward, *J. Mater. Sci.* **1970**, *5*, 909.

[18] F. Shalchy, C. Lovell, A. Bhaskar, *J. Mech. Behav. Biomed. Mater.* **2020**, *110*, 103968.

[19] M. F. Ashby, *Philos. Trans. R. Soc. A* **2006**, *364*, 15.

[20] M. Marvi-Mashhadi, C. Lopes, *Mech. Mater.* **2018**, *124*, 143.

[21] S. Ahn, M. Montero, D. Odell, S. Roundy, P. K. Wright, *Rapid Prototyping J.* **2002**, *8*, 248.

[22] D. W. Hutmacher, T. Schantz, I. Zein, K. W. Ng, S. H. Teoh, K. C. Tan, *J. Biomed. Mater. Res.* **2001**, *55*, 203.

[23] S. Naghieh, M. R. Karamooz Ravari, M. Badrossamay, E. Foroozmehr, M. Kadkhodaei, *J. Mech. Behav. Biomed. Mater.* **2016**, *59*, 241.

[24] J. A. Norato, A. J. Wagoner Johnson, *J. Biomech. Eng.* **2011**, *133*, 091003.

[25] J. M. Sobral, S. G. Caridade, R. A. Sousa, J. F. Mano, R. L. Reis, *Acta Biomater.* **2011**, *7*, 1009.

[26] M. Yeo, C. G. Simon, G. Kim, *J. Mater. Chem. 22*, 21636, **2012**.

[27] S. Arabnejad, D. Pasini, *Int. J. Mech. Sci.* **2013**, *77*, 249.

[28] E. Cuan-Urquizo, A. Bhaskar, *Eur. J. Mech. A* **2018**, *67*, 187.

[29] E. Buckingham, *Phys. Rev.* **1914**, *4*, 345.

[30] G. I. Barenblatt, in *Scaling, Self-Similarity, and Intermediate Asymptotics: Dimensional Analysis and Intermediate Asymptotics*, vol. 14, Cambridge University Press, Cambridge, UK **1996**.

[31] L. Mahadevan, A. Vaziri, M. Das, *EPL* **2007**, *77*, 40003.

[32] A. Bhaskar, K. Jose, *Extreme Mech. Lett.* **2021**, *45*, 101261.

[33] Simulia, Abaqus 6.18 Documentation **2018**.

[34] C. R. Calladine, *Int. J. Solids Struct.* **1977**, *13*, 515.

[35] N. G. Stephen, M. Z. Wang, *J. Appl. Mech.* **1992**, *59*, 747.

[36] J. L. Klemm, R. W. Little, *SIAM J. Appl. Math.* **1970**, *19*, 712.

[37] S. Farah, D. G. Anderson, R. Langer, *Adv. Drug Delivery Rev.* **2016**, *107*, 367.

[38] F. Shalchy, PhD thesis, University of Southampton, **2021**.